3

4

5   **Cofilin-actin rod formation in neuronal processes after brain ischemia**

6

7   Seok Joon Won[1], Angela M. Minnella[1], Long Wu[1], Claire H. Eun[1], Eric Rome[1], Paco S.

8   Herson[2,3], Alisa E. Shaw[4], James R. Bamburg[4], Raymond A. Swanson[1]

9

10   [1] Dept. of Neurology, University of California San Francisco and San Francisco Veterans Affairs

11   Medical Center, San Francisco, CA, USA

12

13   [2] Neuronal Injury Program, Department of Anesthesiology, University of Colorado Anschutz

14   Medical Campus, Aurora, CO, USA.

15

16   [3] Department of Pharmacology, University of Colorado Anschutz Medical Campus, Aurora, CO,

17   USA

18

19   [4] Department of Biochemistry and Molecular Biology, Colorado State University, Fort Collins,

20   CO, USA

21

25

26

27   *To whom correspondence should be sent:

28   Seok Joon Won, Ph.D.

29   Neurology (127), San Francisco Veterans Affairs Medical Center

30   4150 Clement St., San Francisco, CA 94121

31   E-mail: Seokjoon.won@va.gov

32

33

34   Short title: Cofilin-actin rod formation in brain ischemia

Abstract

Functional impairment after brain ischemia results in part from loss of neuronal spines and dendrites, independent of neuronal death. Cofilin-actin rods are covalently linked aggregates of colfilin-1 and actin that form in neuronal processes (neurites) under conditions of ATP depletion and oxidative stress, and which cause neurite degeneration if not disassembled. ATP depletion and oxidative stress occur with differing severity, duration, and time course in different ischemic conditions. Here we evaluated four mouse models of brain ischemia to define the conditions that drive formation of cofilin-actin rods. Three of the models provide early reperfusion: transient middle cerebral artery occlusion (MCAo), transient bilateral common carotid occlusion (CCAo), and cardiac arrest / cardiopulmonary resuscitation (CA/CPR). Early reperfusion restores ATP generating capacity, but also induces oxidative stress. The fourth model, photothrombotic cortical infarction, does not provide reperfusion. Cofilin-actin rods were formed in each of these models, but with differing patterns. Where acute reperfusion occurred, rod formation was maximal within 4 hours after reperfusion. Where infarction occurred, rods continued to form for at least 24 hours after ischemic onset, and extended into the adjacent non-ischemic tissue. Interventions that limit cofilin-actin rod formation may help to preserve integrity of neuronal processes in permanent ischemia.

Key Words: actin, oxidative stress, ischemia, reperfusion, stroke

Introduction

57

58   Neuronal death contributes to functional disability after brain ischemia, and several

59   mechanisms by which this occurs are now well established [1]. Loss of neuronal dendrites and

60   spines may also contribute to functional disability [2-4], but far less is understood about these

61   events. Ischemic injury can induce a loss of spines and dendrites even when the parent neuron

62   survives [3, 4]. This subcellular level of injury is difficult to identify histologically or by standard

63   noninvasive imaging modalities such as magnetic resonance imaging scans. To the extent that

64   dendritic spines represent the anatomical correlate of experience, their loss would be expected

65   to produce a transient, if not permanent functional deficit.

66   One mechanism by which ischemia could injure neurites is through sustained formation of

67   cofilin-actin rods. Cofilin-1 is an actin-binding protein normally involved in the dynamic turnover

68   of actin filaments ("actin treadmilling") and other cell functions [5]. Cofilin-actin rods are formed

69   when cofilin-1 is dephosphorylated by specific phosphatases, the dephosphorylated cofilin-1

70   binds to ADP-actin, and disulfide bonds are generated between the cofilin-1 molecules [6].

71   Oxidative stress, which in brain ischemia is induced through excitotoxic and reperfusion

72   mechanisms, promotes cofilin-actin rod formation by forming intermolecular disulfide bonds

73   between cofilin-1 cysteines 39 and 147 [6-8]. Oxidative stress may also promote rod formation

74   by releasing a cofilin phosphatase, slingshot protein phosphatase-1L (SSH-1L) from its binding

75   protein [9]. In addition, ATP depletion promotes cofilin-actin rod formation by increasing ADP-

76   actin levels and by activating a second cofilin phosphatase, chronophin CIN [10].

77   Cofilin-actin rod formation halts local actin-dependent processes. This can have an

78   immediate energy sparing effect because it interrupts local actin-dependent energy consuming

79   processes such as synaptic vesicle docking and synaptic signaling, spine extension and

80   contraction, dendritic transport, and mitochondrial trafficking [11, 12], and because actin

81   turnover is itself a major source of neuronal energy expenditure [11, 13]. On the other hand,

82   prolonged cessation of actin-mediated processes, such as organelle and protein trafficking, is

83   not compatible with function or survival of neuronal processes [8, 14, 15].

84   Cofilin-actin rods can be imaged using antibodies to cofilin-1, as rod formation condenses the

85   normally dispersed cofilin-1 into readily observable puncta and short rod-like segments.

86   Neurons are the only cell type in brain in which cofilin-actin rods have been definitively localized.

87   The rods form most readily in distal processes, especially dendrites, but can also form in cell

88   bodies [8]. Cofilin-actin rods are biochemically distinct from the actin stress fibers that form in

89   endothelial cells and muscle [16].

90 To our knowledge, there have been no prior published studies of cofilin-actin rod formation in

91 brain ischemia. Ischemic brain injury (ischemic stroke) is broadly classified as either "transient

92 ischemia" (or "ischemia-reperfusion") when reflow occurs soon enough to preserve viability in at

93 least a fraction of the ischemic tissue, or "permanent ischemia" when it does not. ATP depletion

94 and oxidative stress occur with both types of ischemia, but with differing severity, duration, and

95 time courses. Given that both ATP depletion and oxidative stress drive cofilin-actin rod

96 formation, it is difficult to predict the patterns cofilin-actin rod formation that may occur in

97 transient versus permanent ischemia. Accordingly, the aim of this study was to describe the

98 time course and localization of cofilin-actin rod formation in four different mouse brain ischemia

99 models. Three of these models involve reperfusion after variable intervals and somewhat

100 differing anatomical regions of ischemia; transient middle cerebral artery occlusion (MCAo),

101 transient bilateral common carotid occlusion (CCAo), and cardiac arrest / cardiopulmonary

102 resuscitation (CA/CPF). The fourth model, photothrombotic cortical infarction, produces

103 permanent ischemia without reperfusion. Our findings demonstrate robust and extensive

104 formation of cofilin-actin rods in neuronal processes in each of these stroke models, and

105 continued presence of cofilin-actin rods for at least 24 hours in the models that induce infarction.

106

Materials and methods

Animals

109 Studies were approved by the animal studies committees at the San Francisco Veterans

110 Affairs Medical Center, and the University of Colorado, and were performed in accordance with

111 the National Institutes of Health Guide for the Care and Use of Laboratory Animals. Results are

112 reported in accordance with the ARRIVE guidelines [17]. Reagents were obtained from Sigma

113 Aldrich, St. Louis, where not otherwise noted.

114

Cell Culture studies

116 Mixed neuron-astrocyte cultures were prepared from the cortices of embryonic day 16 mice

117 of both sexes and plated on poly-D-lysine coated glass coverslips. After 4 days in culture, 1.2

118 μM cytosine arabinoside was added to culture media to suppress astrocyte proliferation. The

119 cells were subsequently maintained in NeuroBasal medium (Gibco) containing 5% fetal bovine

120 serum and 5 mM glucose, and used at day 13-15 in vitro. Experiments were initiated by

121 exchanging the culture medium with a balanced salt solution (BSS): 1.2 mM $CaCl_2$, 0.4 mM

122 $MgSO_4$, 5.3 mM KCl, 0.4 mM KH_2PO_4, 137 mM $NaCl_2$, 0.3 mM $NaHPO_4$, 5 mM glucose, and 10

123 mM 1,4-piperazinediethanesulfonate (PIPES) buffer, pH 7.3. Chemical oxygen-glucose

124 deprivation (cOGD) was induced by adding 6 mM 2-deoxyglucose and 10 mM sodium azide to

125 the BSS. After 20 minutes incubation at 37 °C, both the control BSS and cOGD BSS were

126 replaced by fresh BSS, and after an additional 10 minutes incubation the cultures were fixed

127 with phosphate-buffered 4% formaldehyde. Each experiment was performed on an independent

128 culture preparation and included 4 replicates per condition.

129

Transient focal cerebral ischemia

131 Adult (age 3-4 months) male C57BL6 mice were anesthetized with 2% isoflurane in 70%

132 N_2O/ balance O_2 delivered through a ventilated nose cone. Rectal temperature was maintained

133 at 37 ± 0.5 °C using a homeothermic blanket throughout the surgical procedure. Transient

134 ischemia in the middle cerebral artery (MCA) distribution was induced by the Weinstein

135 intraluminal filament method [18, 19]. The right common carotid artery was exposed through a

136 midline incision, separated from the vagus nerve, and temporarily ligated. The distal part of

137 external carotid artery was ligated, and a silicon-coated 6-0 monofilament (Doccol Corporation,

138 Sharon, MA) was inserted through the proximal external common carotid artery stump and

139 advanced along the internal carotid artery until the tip occluded the proximal stem of the MCA.

140 Regional cerebral blood flow was monitored using Laser Doppler Flowmetry (Moor instruments

141 Ltd, UK). After 30 minutes of occlusion, blood flow was restored by removal of the

142 monofilament. The wound was sutured, bupivacaine (6 mg/kg) and meloxicam (7.5 mg/kg) were

143 administered subcutaneously, and the mouse was moved to warmed recovery chamber until

144 awake and ambulatory. For sham surgery, mice were subjected to the same procedure but

145 without intraluminal suture insertion. Mice were excluded from the study if the measured

146 cerebral blood flow was not reduced by more than 70% during vessel occlusion.

147

Transient forebrain ischemia

149 Adult (age 3-4 months) male C57BL6 mice were anesthetized with 2% isoflurane in 70%

150 N_2O/ balance O_2, delivered through a ventilated nose cone. Rectal temperature was maintained

151 at 37 ± 0.5 °C by using a homeothermic blanket throughout the surgical procedure. Forebrain

152 global ischemia was induced by occluding both common carotid arteries as described previously

153 [20, 21]. The common carotid arteries (CCAs) were exposed bilaterally and isolated from the

154 adjacent vagus nerves. Microvascular clips were applied to both CCAs. After 16 minutes of

155   occlusion, clips were removed and patency of each CCA was confirmed by inspection under the

156   surgical microscope. The wound was sutured, bupivacaine (6 mg/kg) and meloxicam (7.5

157   mg/kg) were administered subcutaneously, and the mouse was moved to warmed recovery

158   chamber until awake and ambulatory. Sham-operated animals received the same neck skin

159   incision but artery occlusion was not performed. Mice were excluded from analysis if

160   reperfusion was not observed in both CCAs, or if mice developed seizures.

161

Photothrombotic permanent ischemia

163   Adult (age 3-4 months) male C57BL6 mice were anesthetized with 2% isoflurane in 70%

164   N_2O/ balance O_2, delivered through a ventilated nose cone. Rectal temperature was maintained

165   at 37 ± 0.5 °C by using a homeothermic blanket throughout the surgical procedure.

166   Photothrombotic permanent ischemia was induced by the Rose Bengal technique [22, 23]. A

167   PE10 polyethylene catheter (Becton Dickinson, Franklin, NJ) was introduced into the femoral

168   vein, and the head was immobilized in a stereotaxic frame. The skull was exposed by skin

169   incision, and a 2 mm diameter fiber optic cable was place on the skull 1.0 mm anterior, and 1.5

170   mm lateral to bregma. Rose Bengal (Sigma-Aldrich, St Louis, MO; 20 mg/kg) dissolved in saline

171   was infused through the venous cannula for 1 minute, and vascular occlusion was induced by

172   10 minutes illumination with white light (KL 1500 LCD, SCHOTT North America Inc.,

173   Southbridge, MA) through the fiber optic cable. Sham ischemia animals were injected with

174   saline only but were otherwise treated identically. The incisions were sutured, bupivacaine (6

175   mg/kg) and meloxicam (7.5 mg/kg) were administered subcutaneously, and the mouse was

176   moved to warmed recovery chamber until awake and ambulatory.

177

Cardiac arrest / cardiopulmonary resuscitation

179   These studies were approved by the University of Colorado Institutional Animal Care and

180   Use Committee. Adult (age 3-4 months) male C57BL6 mice were subjected to CA/CPR as

181   previously described [24, 25]. Anesthesia was induced with 3% isoflurane and maintained with

182   1.5–2% isoflurane in oxygen enriched air via facemask. Temperature probes were inserted in

183   the left ear and rectum to monitor head and body temperature simultaneously. A PE-10 catheter

184   was inserted into the right internal jugular vein for drug administration. Needle electrodes were

185   placed subcutaneously on the chest for continuous EKG monitoring. Animals were

186   endotracheally intubated and connected to a mouse ventilator. Cardiac arrest was induced by

187   injection of 50 µL KCl (0.5M) via the jugular catheter and confirmed by asystole on EKG. The

6

188   endotracheal tube was disconnected and anesthesia stopped. During cardiac arrest, body

189   temperature was allowed to spontaneously decrease to a minimum of 35.5 °C, and head

190   temperature was maintained at 37.5 °C. Resuscitation was begun 8 min after induction of

191   cardiac arrest by injection of 0.05–0.10 ml epinephrine solution (16 µg epinephrine/ml 0.9%

192   saline), chest compressions, and ventilation with 100% oxygen at a respiratory rate of 200/min

193   and 25% greater tidal volume. Chest compressions were stopped when spontaneous circulation

194   was restored. Resuscitation was abandoned if spontaneous circulation was not restored within

195   2.5 min. Both catheters and temperature probes were then removed and skin wounds closed.

196

Histology and immunocytochemistry

198   Anesthetized mice were perfused with cold saline (0.9% NaCl) followed by saline containing

199   phosphate-buffered 4% formaldehyde (PFA). After post-fixation with 4% PFA for 24 hours,

200   brains were immersed for another 24 hours in 20% sucrose for cryoprotection. The brains were

201   then frozen and 40 µm coronal sections were prepared with a cryostat. The sections were

202   permeablized with 95% methanol and 5% 0.1 M phosphate buffer for 15 minutes at -20 °C, then

203   washed with phosphate-buffered saline. The fixed brain sections were pre-incubated in blocking

204   buffer (2% donkey serum and 0.1% bovine serum albumin in 0.1 M phosphate buffer) at room

205   temperature for 30 minutes, and then incubated with primary antibody overnight at 4 °C. After

206   washing, the sections were incubated with fluorescent secondary antibody (Life Technologies

207   Corporation, Grand Island, NY; 1:500) for one hour at room temperature. Where double labeling

208   was additionally performed with cell-type specific antibodies, the sections were subsequently

209   incubated with blocking buffer additionally containing 0.3% Triton X-100, and then incubated

210   with those antibodies overnight at 4 °C followed by appropriate fluorescent secondary

211   antibodies. Stained sections were mounted on glass slides in DAPI-containing mounting

212   medium (Vector laboratories, Burlingame, CA). Control sections were prepared omitting either

213   primary or secondary antibodies. Immunostaining of cell cultures was done identically except

214   that incubation time with primary antibody was shortened to 6 hours.

215   Primary antibodies were obtained from the following sources and used at the designated

216   dilutions: rabbit anti-cofilin-1, Cytoskeleton #ACFL02, Denver, CO (1:250); mouse anti-MAP2,

217   Millipore #3418, Temecula, CA (1:1000); mouse anti-NeuN, Millipore #MAB377, Temecula, CA

218   (1:1000); mouse anti-NF-H, BioLegend #SMI31, San Diego, CA (1:2000); goat anti-APP, Abcam

219   #Ab2084, Cambridge, MA (1:400); mouse anti-CNPase, Promega #G346A, Madison, WI

220   (1:800); mouse anti-GFAP, Millipore #MAB360, Temecula, CA (1:1000); goat anti-CD3,

221   BioTechne #AF3628, Minneapolis, MN (1:200); rat anti-CD11b, BioRad # MCA711, Hercules,

222 CA (1:250); mouse anti-mouse IgG, Vector Lab #AI-9200, Burlingame, CA (1:250). Mouse anti-

223 cofilin1 #mAb22 (1:300) and rabbit anti- pospho-3-serine cofilin-1 # 4321 (1:2500) were

224 provided by J. R. Bamburg, Colorado State University [26, 27].

225

Image analysis of cofilin-actin rod formation

227 Confocal images were taken at three pre-determined locations on three sections from each

228 animal. For photothrombotic stroke, this area was at the lateral edge of the ischemic cortical

229 region. This region was difficult to define by visual inspection alone at the 1 and 4 hour time

230 points, and for brains harvested at these time points the ischemic territory was identified by

231 immunostaining for IgG, which is trapped in the vessels of the photo-thrombosed territory and

232 not washed out during perfusion-fixation.   The confocal images were z-stacked using the NIH

233 ImageJ program and used for quantifying cofilin-1 immunoreactivity. Each processed image

234 was prepared using a stack of 10, 1 µm Z-stage images (10 µm thickness). Background signal

235 was defined as the signal level that excluded approximately 98% of pixels in a non-ischemic

236 brain region from each section. This threshold was then applied to the ischemic region of

237 interest, and the area of ischemia-induced cofilin signal was measured and expressed as

238 percent of the image area (for brain sections) or percent of the MAP2 staining area (for cell

239 cultures). Values for each image were averaged to provide an aggregate value for each brain.

240 Both the person taking the photographs and the person analyzing the immunostaining were

241 blinded to the treatment conditions.

242

Image analysis of total cofilin-1 and ser-3-phospho-cofilin-1

244 Neuron cultures or brain sections were doubled labeled using rabbit antibody targeting

245 serine-3-phospho-cofilin-1 [28] and mouse antibody targeting total cofilin-1 [29]. The signal from

246 each antibody was assessed along 2 µm line segments oriented orthogonal to the axes of

247 individual neurites. These segments were placed over sites of cofilin-actin rod formation in

248 neurons treated with cOGD, and over non-rod-containing neurites in control cultures. (More than

249 95% of neurites had no rods in the control condition.) A background subtraction was made for

250 each antibody signal using values obtained where no cells were present. The peak value of

251 each of these determinations was used for aggregate statistical analysis. For assessments in

252 brain sections, confocal images were taken in the peri-infarct regions of sections from 3 animals

253 and a total of 29 cofilin-actin rods were selected for quantification using the same method as

254 used for cultured cells, but without background subtraction.

255

Statistics

257   All data are expressed as means ± s.e.m., with the "n" of each study defined as the number

258   of mice or, for cell cultures, the number of independent experiments unless otherwise stated.

259   Data were analyzed using one-way ANOVA and the Dunnett's test for multiple comparisons

260   against a common (control) group. Where only two groups were compared, the two-sided t-test

261   was used.

262

Results

264   We first validated cofilin-actin rod detection using a cell culture model of stroke, in which

265   energy failure is induced by blocking glucose and oxygen utilization (chemical oxygen-glucose

266   deprivation; cOGD). cOGD induced widespread formation of punctate and rod-shaped

267   aggregates in neuronal processes that were recognized by rabbit antibody to cofilin-1 (Fig 1).

268   These aggregates are characteristic of cofilin-actin rods [30, 31] were localized primarily to the

269   neurites, though some were also observed in cell soma. Some neurites contained segments in

270   which the rods were co-localized with microtubule-associated protein-2 (MAP2), whereas other

271   segments showed an abrupt discontinuity of MAP2 at sites of rod formation (Fig 1). This pattern

272   is in agreement with prior studies showing disruption of the neurite cytoskeleton by cofilin-actin

273   rod formation [31-33]. Rare foci of cofilin-1 aggregation were also observed in control cultures

274   that were treated with medium exchanges only.

275   We next evaluated cofilin-actin rod formation in mice exposed to the transient MCAo model

276   of stroke, using brains harvested 1, 4 and 24 hours after reperfusion. Transient MCAo produces

277   a central core of near-zero blood flow, and a surrounding penumbral region with less severe

278   ischemia [34]. Using this stroke model, we found no significant cofilin-actin rod formation at one-

279   hour time post-reperfusion, but widespread formation at both the 4- and 24-hour time points (Fig

280   2). Sections from the 24-hour reperfusion group were then double-labeled for cofilin-1 and cell-

281   type specific markers. The cofilin-1 immunostaining was restricted to cellular elements with the

282   morphology and size of neuronal processes, and as in the cell culture studies some processes

283   showed an abrupt discontinuity of cytoskeletal markers (MAP2 and NF-H) (Fig 3). The higher

284   magnification views also show that many of the cofilin-actin rods that appear non-linear are

285   composed of overlapping linear arrays. This is best seen in neurons co-labeled with the axonal

286   marker amyloid precursor protein (APP), which is not a cytoskeletal element. By contrast, there

287   was no co-localization between cofilin-1 and either the oligodendrocyte marker CNPase, the

288   astrocyte cytoskeletal marker GFAP, the microglia/macrophage marker CD11b, or the

289   endothelial cell marker CD31 (cluster of differentiation 31; also termed platelet endothelial cell

290   adhesion molecule-1) (Fig 3).

291   We next evaluated cofilin-actin rod formation in the transient bilateral carotid artery

292   occlusion (CCAo) of stroke. In mice, CCAo produces neuronal death preferentially in the

293   forebrain cortex and in the hippocampal CA1 and dentate gyrus [20]. The neuronal death can

294   be significantly attenuated by NMDA receptor antagonists or NADPH oxidase inhibition during

295   reperfusion[21, 35, 36], indicating significant oxidative stress in these regions during ischemia-

296   reperfusion. Immunostaining for cofilin-1 after CCAo showed rod shaped and punctate

297   accumulation predominately in these same anatomical regions (Fig 4a). The morphology of

298   cofilin-actin rods was similar to that observed after MCAo, but the time course was different. In

299   CA1 and cortex, the extent of rod formation was several-fold greater than control by 1 hour after

300   reperfusion, but less at 24 hours (Fig 4b). The pattern was different in the dentate gyrus, with

301   peak signal observed at the zero time point (immediately before reperfusion, when ATP levels

302   are likely lowest), and had resolved by 1 hour.

303   We additionally evaluated brains from mice subjected to cardiac arrest / cardiopulmonary

304   resuscitation (CA/CPR) [24, 25]. CA/CPR renders the entire brain ischemic, but for a shorter

305   interval than the CCAo model. Brains from CA/CPR mice showed negligible cofilin-actin rod

306   formation in cortex (not shown), perhaps reflecting the shorter ischemic duration. Rod formation

307   was observed in the in the hippocampal dentate gyrus and CA1 (Fig 5), though less extensively

308   than in the CCAo mice.

309   Most clinical strokes are caused by emboli that persist for many hours or days, and hence

310   may better be mimicked by permanent ischemia animal models that do not provide early

311   reperfusion. To evaluate cofilin-actin rod formation in permanent ischemia, we used a

312   photothrombotic method to induce infarction in a defined region of mouse cortex (Fig 6a).

313   Cofilin-actin rods were identified primarily on the border region of the resulting infarct, and not in

314   the infarct core (Fig 6b,c). In contrast to the stroke models with early reperfusion, rod formation

315   was observed to increase between 1 and 24 hours after ischemia onset, and expand out into

316   the non-ischemic tissue in which normal cell nuclei were apparent (Fig 6d).

317   Cofilin-actin rod formation requires de-phosphorylation of the serine-3 residue of cofilin-1.

318   Thus, to further confirm the nature of the aggregates detected by cofilin-1 immunostaining, we

319   used neuron cultures exposed to cOGD and then probed these with antibodies that target either

320   total cofilin-1 or specifically ser-3-phosphocofilin-1 [26, 28, 29]. The antibody recognizing 3-ser-

321   phosphocofilin was generated in rabbit, and consequently a mouse antibody to total cofilin-1

322   was used to perform the double labeling. As shown Fig 7a, the mouse antibody to total cofilin-1

323   showed the same pattern of rod formation after cOGD as observed with the rabbit antibody to

324   total cofilin-1 in Fig 1. Double labeling for ser-3-phosphocofilin-1 showed globally reduced

325   immunoreactivity in cOGD-treated neurons, along with a striking reduction in the ratio of ser-3-

326   phosphocofilin-1: total cofilin-1 at sites of cofilin-actin rod formation. This double-labeling

327   approach was then used to similarly assess post-ischemic brain sections. As shown in Fig 7d,e

328   a reduction in the ratio of ser-3-phosphocofilin-1 : total cofilin-1 was also observed at sites of

329   ischemia-induced cofilin-actin rod formation *in vivo*. The magnitude of this reduction appeared

330   to be less than in the cell cultures, possibly because of signal from tissue above and below the

331   selected neurites (despite confocal imaging) or partial re-phosphorylation of free cofilin-1 in the

332   24 hour interval between ischemia and brain harvest.

333

Discussion

335   Our primary aim was to describe and compare cofilin-actin rod formation in established

336   brain ischemia models that produce differing components of reperfusion injury. For technical

337   reasons it was not possible to evaluate uniform time points in each ischemia model, but

338   nevertheless several distinct patterns emerge from these studies. First, the two models with

339   brief ischemic intervals, CCAo and cardiac arrest, both induced rods preferentially in areas

340   known to exhibit high levels of oxidative stress with ischemia-reperfusion; the hippocampal CA1

341   and dentate gyrus. In both of these models rod formation was maximal within 3 hours of

342   reperfusion and had largely resolved at later time points. By contrast, the two models causing

343   frank infarction (MCAo and photothrombosis) both produced a progressive increase in rod

344   formation over the 24 hour observation interval. The photothrombotic model uniquely permits

345   clear delineation of the ischemic border, and here rod formation was found to extend into the

346   non-ischemic territory at the 24 hour time point. Importantly, rod formation was not observed in

347   the core of the photothrombotic stroke, indicating that it is not simply an inevitable aspect of

348   neuronal death. Notably, in all four stroke models cofilin-actin rod formation was significant long

349   before neuronal degeneration occurs.

350   Cell culture studies have shown that oxidative stress promotes cofilin-actin rod formation

351   through effects on cofilin phosphorylation state and intermolecular disulfide bonding [6-8]. Our

352   findings indirectly support oxidative stress as a major factor promoting rod formation in brain

353   ischemia. Oxidative stress is induced in transient ischemia by reperfusion of oxygenated blood,

354   and at the margins of permanent ischemia by excitotoxicity. Here, brain ischemia induced rod

355   formation in regions of reperfusion, and at the edge (but not core) of the permanent

356   photothrombotic lesions.

357   Support for a specifically neuronal localization of the cofilin-actin rods in these studies is

358   provided by the size and morphology of the cofilin-immunoreactive structures, the lack of co-

359   localization with other cell-type specific markers, the presence of cofilin-actin rods in processes

360   contiguous with neuron-specific markers, and their similar appearance to those produced in

361   neuronal cultures treated with cOGD. The anti-cofilin antibodies used for these studies have

362   been extensively characterized in neurons and other cell types [26-29]. The antibody against

363   phosphoserine 3 of cofilin-1 also recognizes the phosphorylated serine 3 of the closely related

364   protein ADF (actin depolymerizing protein); but ADF is present low levels relative to cofilin-1 in

365   mouse neurons cells [26]. The culture studies presented here were performed primarily to

366   validate the reagents used for cofilin-actin rod detection, but they additionally show MAP2-

367   postive neurites containing discrete segments of cofilin-actin rod formation and disrupted MAP2

368   signal. This same pattern was observed *in vivo* following ischemia, further supporting a

369   specifically neuronal localization of cofilin-actin rod formation. The reason why rod formation

370   causes cytoskeletal disruption is not known, but may be related to actin sequestration in rods

371   and cessation of normal transport along neuronal processes [14, 31, 32, 37].

372   Evidence suggests that rod formation reduces energy expenditure over short time

373   intervals, but leads to neurite degeneration if sustained [6-8]. Given that energy failure is a

374   primary initiator ischemic cell death, the formation of cofilin-actin rods could have either

375   beneficial or deleterious effects on neurite survival depending upon ischemia duration and other

376   factors. It is also possible that rod formation in neurites contributes to the survival (or death) of

377   the parent neuron either through energy-related processes or other recognized mechanisms

378   [38].

379   The exploratory design of this study required some limitations. In order to evaluate multiple

380   time points in each of four stroke models, we used small numbers of mice at each time point,

381   and used only adult male mice to minimize variability within each treatment condition. It is

382   possible that age or sex may influence rod formation or resolution in ways that differ from the

383   patterns observed here. Most importantly, these descriptive findings do not establish whether

384   cofilin-actin rod formation has a causal effect on cell or neurite survival, or on long term

385   functional outcomes. Tests of these potential cause-effect relationships will require studies in

386   which rod formation is suppressed or promoted. Reagents are now becoming available to this

387   end [39-41], and the observations presented here should help provide a framework for such

388   efforts.

389 # Acknowledgements

399

400

References

1. Moskowitz MA, Lo EH, Iadecola C. The science of stroke: mechanisms in search of treatments. Neuron. 2010;67(2):181-98. Epub 2010/07/31. doi: S0896-6273(10)00540-4 [pii] 10.1016/j.neuron.2010.07.002. PubMed PMID: 20670828.

2. Neumann JT, Cohan CH, Dave KR, Wright CB, Perez-Pinzon MA. Global cerebral ischemia: synaptic and cognitive dysfunction. Curr Drug Targets. 2013;14(1):20-35. PubMed PMID: 23170794.

3. Zhang S, Boyd J, Delaney K, Murphy TH. Rapid reversible changes in dendritic spine structure in vivo gated by the degree of ischemia. J Neurosci. 2005;25(22):5333-8. doi: 10.1523/JNEUROSCI.1085-05.2005. PubMed PMID: 15930381.

4. Brown CE, Wong C, Murphy TH. Rapid morphologic plasticity of peri-infarct dendritic spines after focal ischemic stroke. Stroke. 2008;39(4):1286-91. doi: 10.1161/STROKEAHA.107.498238. PubMed PMID: 18323506.

5. Kanellos G, Frame MC. Cellular functions of the ADF/cofilin family at a glance. J Cell Sci. 2016;129(17):3211-8. doi: 10.1242/jcs.187849. PubMed PMID: 27505888.

6. Bernstein BW, Shaw AE, Minamide LS, Pak CW, Bamburg JR. Incorporation of cofilin into rods depends on disulfide intermolecular bonds: implications for actin regulation and neurodegenerative disease. J Neurosci. 2012;32(19):6670-81. Epub 2012/05/11. doi: 10.1523/jneurosci.6020-11.2012. PubMed PMID: 22573689; PubMed Central PMCID: PMCPmc3745285.

7. Bernstein BW, Bamburg JR. ADF/cofilin: a functional node in cell biology. Trends Cell Biol. 2010;20(4):187-95. doi: 10.1016/j.tcb.2010.01.001. PubMed PMID: 20133134; PubMed Central PMCID: PMCPMC2849908.

8. Bamburg JR, Bernstein BW. Actin dynamics and cofilin-actin rods in alzheimer disease. Cytoskeleton (Hoboken). 2016;73(9):477-97. doi: 10.1002/cm.21282. PubMed PMID: 26873625; PubMed Central PMCID: PMCPMC5345344.

9. Kim JS, Huang TY, Bokoch GM. Reactive oxygen species regulate a slingshot-cofilin activation pathway. Mol Biol Cell. 2009;20(11):2650-60. Epub 2009/04/03. doi: 10.1091/mbc.E09-02-0131. PubMed PMID: 19339277; PubMed Central PMCID: PMCPmc2688545.

10. Huang TY, Minamide LS, Bamburg JR, Bokoch GM. Chronophin mediates an ATP-sensing mechanism for cofilin dephosphorylation and neuronal cofilin-actin rod formation.

14

433   Dev Cell. 2008;15(5):691-703. doi: 10.1016/j.devcel.2008.09.017. PubMed PMID: 19000834;
434   PubMed Central PMCID: PMCPMC2644054.

435   11.   Bernstein BW, Bamburg JR. Actin-ATP hydrolysis is a major energy drain for neurons. J
436   Neurosci. 2003;23(1):1-6. PubMed PMID: 12514193.

437   12.   Bernstein BW, Chen H, Boyle JA, Bamburg JR. Formation of actin-ADF/cofilin rods
438   transiently retards decline of mitochondrial potential and ATP in stressed neurons. Am J
439   Physiol Cell Physiol. 2006;291(5):C828-39. doi: 10.1152/ajpcell.00066.2006. PubMed PMID:
440   16738008.

441   13.   Engl E, Attwell D. Non-signalling energy use in the brain. J Physiol. 2015;593(16):3417-
442   29. doi: 10.1113/jphysiol.2014.282517. PubMed PMID: 25639777; PubMed Central PMCID:
443   PMCPMC4560575.

444   14.   Cichon J, Sun C, Chen B, Jiang M, Chen XA, Sun Y, et al. Cofilin aggregation blocks
445   intracellular trafficking and induces synaptic loss in hippocampal neurons. J Biol Chem.
446   2012;287(6):3919-29. doi: 10.1074/jbc.M111.301911. PubMed PMID: 22184127; PubMed
447   Central PMCID: PMCPMC3281697.

448   15.   Bamburg JR, Bernstein BW, Davis RC, Flynn KC, Goldsbury C, Jensen JR, et al.
449   ADF/Cofilin-actin rods in neurodegenerative diseases. Curr Alzheimer Res. 2010;7(3):241-
450   50. Epub 2010/01/22. PubMed PMID: 20088812; PubMed Central PMCID:
451   PMCPmc4458070.

452   16.   Shi Y, Zhang L, Pu H, Mao L, Hu X, Jiang X, et al. Rapid endothelial cytoskeletal
453   reorganization enables early blood-brain barrier disruption and long-term ischaemic
454   reperfusion brain injury. Nat Commun. 2016;7:10523. doi: 10.1038/ncomms10523. PubMed
455   PMID: 26813496; PubMed Central PMCID: PMCPMC4737895.

456   17.   Kilkenny C, Browne WJ, Cuthill IC, Emerson M, Altman DG. Improving bioscience
457   research reporting: the ARRIVE guidelines for reporting animal research. PLoS Biol.
458   2010;8(6):e1000412. doi: 10.1371/journal.pbio.1000412. PubMed PMID: 20613859; PubMed
459   Central PMCID: PMCPMC2893951.

460   18.   Sheth SA, Iavarone AT, Liebeskind DS, Won SJ, Swanson RA. Targeted Lipid Profiling
461   Discovers Plasma Biomarkers of Acute Brain Injury. PLoS One. 2015;10(6):e0129735. doi:
462   10.1371/journal.pone.0129735. PubMed PMID: 26076478; PubMed Central PMCID:
463   PMC4468135.

464 19. Longa EZ, Weinstein PR, Carlson S, Cummins R. Reversible middle cerebral artery

465   occlusion without craniectomy in rats. Stroke. 1989;20(1):84-91. PubMed PMID:

466   0002643202.

467 20. Smith ML, Bendek G, Dahlgren N, Rosen I, Wieloch T, Siesjo BK. Models for studying

468   long-term recovery following forebrain ischemia in the rat. 2. A 2-vessel occlusion model.

469   Acta Neurol Scand. 1984;69(6):385-401. PubMed PMID: 6464670.

470 21. Won SJ, Kim JE, Cittolin-Santos GF, Swanson RA. Assessment at the single-cell level

471   identifies neuronal glutathione depletion as both a cause and effect of ischemia-reperfusion

472   oxidative stress. J Neurosci. 2015;35(18):7143-52. doi: 10.1523/JNEUROSCI.4826-14.2015.

473   PubMed PMID: 25948264; PubMed Central PMCID: PMC4420782.

474 22. Watson BD, Dietrich WD, Busto R, Wachtel MS, Ginsberg MD. Induction of reproducible

475   brain infarction by photochemically initiated thrombosis. Ann Neurol. 1985;17(5):497-504.

476   doi: 10.1002/ana.410170513. PubMed PMID: 4004172.

477 23. Gulati T, Won SJ, Ramanathan DS, Wong CC, Bodepudi A, Swanson RA, et al. Robust

478   neuroprosthetic control from the stroke perilesional cortex. J Neurosci. 2015;35(22):8653-61.

479   doi: 10.1523/JNEUROSCI.5007-14.2015. PubMed PMID: 26041930.

480 24. Kofler J, Hattori K, Sawada M, DeVries AC, Martin LJ, Hurn PD, et al. Histopathological

481   and behavioral characterization of a novel model of cardiac arrest and cardiopulmonary

482   resuscitation in mice. J Neurosci Methods. 2004;136(1):33-44. doi:

483   10.1016/j.jneumeth.2003.12.024. PubMed PMID: 15126043.

484 25. Quillinan N, Deng G, Shimizu K, Cruz-Torres I, Schroeder C, Traystman RJ, et al. Long-

485   term depression in Purkinje neurons is persistently impaired following cardiac arrest and

486   cardiopulmonary resuscitation in mice. J Cereb Blood Flow Metab. 2017;37(8):3053-64. doi:

487   10.1177/0271678X16683691. PubMed PMID: 28168893; PubMed Central PMCID:

488   PMCPMC5536809.

489 26. Garvalov BK, Flynn KC, Neukirchen D, Meyn L, Teusch N, Wu X, et al. Cdc42 regulates

490   cofilin during the establishment of neuronal polarity. J Neurosci. 2007;27(48):13117-29. doi:

491   10.1523/JNEUROSCI.3322-07.2007. PubMed PMID: 18045906.

492 27. Flynn KC, Pak CW, Shaw AE, Bradke F, Bamburg JR. Growth cone-like waves transport

493   actin and promote axonogenesis and neurite branching. Dev Neurobiol. 2009;69(12):761-79.

494   doi: 10.1002/dneu.20734. PubMed PMID: 19513994; PubMed Central PMCID:

495   PMCPMC2845293.

496   28.   Meberg PJ, Ono S, Minamide LS, Takahashi M, Bamburg JR. Actin depolymerizing factor
497   and cofilin phosphorylation dynamics: response to signals that regulate neurite extension.
498   Cell Motil Cytoskeleton. 1998;39(2):172-90. doi: 10.1002/(SICI)1097-
499   0169(1998)39:2<172::AID-CM8>3.0.CO;2-8. PubMed PMID: 9484959.

500   29.   Abe H, Ohshima S, Obinata T. A cofilin-like protein is involved in the regulation of actin
501   assembly in developing skeletal muscle. J Biochem. 1989;106(4):696-702. PubMed PMID:
502   2691511.

503   30.   Minamide LS, Maiti S, Boyle JA, Davis RC, Coppinger JA, Bao Y, et al. Isolation and
504   characterization of cytoplasmic cofilin-actin rods. J Biol Chem. 2010;285(8):5450-60. Epub
505   2009/12/22. doi: 10.1074/jbc.M109.063768. PubMed PMID: 20022956; PubMed Central
506   PMCID: PMCPmc2820773.

507   31.   Minamide LS, Striegl AM, Boyle JA, Meberg PJ, Bamburg JR. Neurodegenerative stimuli
508   induce persistent ADF/cofilin-actin rods that disrupt distal neurite function. Nat Cell Biol.
509   2000;2(9):628-36. Epub 2000/09/12. doi: 10.1038/35023579. PubMed PMID: 10980704.

510   32.   Whiteman IT, Gervasio OL, Cullen KM, Guillemin GJ, Jeong EV, Witting PK, et al.
511   Activated actin-depolymerizing factor/cofilin sequesters phosphorylated microtubule-
512   associated protein during the assembly of alzheimer-like neuritic cytoskeletal striations. J
513   Neurosci. 2009;29(41):12994-3005. doi: 10.1523/JNEUROSCI.3531-09.2009. PubMed
514   PMID: 19828813; PubMed Central PMCID: PMCPMC2821881.

515   33.   Whiteman IT, Minamide LS, Goh de L, Bamburg JR, Goldsbury C. Rapid changes in
516   phospho-MAP/tau epitopes during neuronal stress: cofilin-actin rods primarily recruit
517   microtubule binding domain epitopes. PLoS One. 2011;6(6):e20878. doi:
518   10.1371/journal.pone.0020878. PubMed PMID: 21738590; PubMed Central PMCID:
519   PMCPMC3125162.

520   34.   Traystman RJ. Animal models of focal and global cerebral ischemia. ILAR J.
521   2003;44(2):85-95. PubMed PMID: 12652003.

522   35.   Meldrum BS, Evans MC, Swan JH, Simon RP. Protection against hypoxic/ischaemic brain
523   damage with excitatory amino acid antagonists. Med Biol. 1987;65(2-3):153-7. PubMed
524   PMID: 2888931.

525   36.   Wang Q, Tompkins KD, Simonyi A, Korthuis RJ, Sun AY, Sun GY. Apocynin protects
526   against global cerebral ischemia-reperfusion-induced oxidative stress and injury in the gerbil
527   hippocampus. Brain Res. 2006;1090(1):182-9. PubMed PMID: 16650838.

528   37.   Mi J, Shaw AE, Pak CW, Walsh KP, Minamide LS, Bernstein BW, et al. A genetically

529   encoded reporter for real-time imaging of cofilin-actin rods in living neurons. PLoS One.

530   2013;8(12):e83609. Epub 2014/01/07. doi: 10.1371/journal.pone.0083609. PubMed PMID:

531   24391794; PubMed Central PMCID: PMCPmc3877059.

532   38.   Liu T, Wang F, LePochat P, Woo JA, Bukhari MZ, Hong KW, et al. Cofilin-mediated

533   Neuronal Apoptosis via p53 Translocation and PLD1 Regulation. Sci Rep. 2017;7(1):11532.

534   doi: 10.1038/s41598-017-09996-3. PubMed PMID: 28912445; PubMed Central PMCID:

535   PMCPMC5599510.

536   39.   Alhadidi Q, Bin Sayeed MS, Shah ZA. Cofilin as a Promising Therapeutic Target for

537   Ischemic and Hemorrhagic Stroke. Transl Stroke Res. 2016;7(1):33-41. doi:

538   10.1007/s12975-015-0438-2. PubMed PMID: 26670926.

539   40.   Madineni A, Alhadidi Q, Shah ZA. Cofilin Inhibition Restores Neuronal Cell Death in

540   Oxygen-Glucose Deprivation Model of Ischemia. Mol Neurobiol. 2016;53(2):867-78. doi:

541   10.1007/s12035-014-9056-3. PubMed PMID: 25526862; PubMed Central PMCID:

542   PMCPMC4475502.

543   41.   Shaw AE, Bamburg JR. Peptide regulation of cofilin activity in the CNS: A novel

544   therapeutic approach for treatment of multiple neurological disorders. Pharmacol Ther.

545   2017;175:17-27. doi: 10.1016/j.pharmthera.2017.02.031. PubMed PMID: 28232023; PubMed

546   Central PMCID: PMCPMC5466456.

547

548

549

550

551

Figure legends

Fig 1. Oxygen-glucose deprivation induces formation of cofilin-actin rods in cultured neurons.

a. Neurons are immunostained using antibodies to cofilin-1 (red) and MAP2 (green), with nuclei stained blue with DAPI. Cultures were treated for 30 minutes with chemical oxygen-glucose deprivation (cOGD) or medium exchanges only (control). **b**. Oval in enlarged view identifies a segment of neuronal process in which cofilin-actin rods have formed and MAP2 immunoreactivity is lost. C. Graph quantifies the relative area of cofilin staining in the control and cOGD conditions, expressed as percent of the area of MAP2 immunoreactivity. n = 4; **p < 0.01.

Fig 2. Cofilin-actin rod formation after transient focal ischemia

a. Lesioned area as identified by NeuN immunostaining in brain fixed 24 hours after a 30-minute MCA occlusion. Blue line marks the approximate medial edge of the lesion, and blue box shows the area photographed on each section after cofilin-1 immunostaining. **b**. Immunostaining for cofilin-1 (red) in the ischemic cortex at designated time points after reperfusion. Cell nuclei are stained blue. **c**. Graph quantifies area of cofilin staining at each time point, expressed as percent of the image area (n = 3-4; *p < 0.05 v. sham).

Fig 3. Cofilin-actin rods form in neurons

Panels show double immunostaining for cofilin-1 (red) and cell-type specific markers for neurons (MAP2 and NF-H), neuronal axons (APP), oligodendrocytes (CNPase), astrocytes (GFAP), microglia/macrophages (CD11b) and endothelial cells (CD31). Cell nuclei are stained blue. Yellow boxes denote the areas magnified in adjacent panels. Cofilin aggregates were observed in neuronal dendrites and axons (arrows) but not in other cell types. Brain sections were from ischemic cortex collected 24 hours after 30 minutes MCA occlusion and are representative of n = 4 mice.

Fig 4. Cofilin-actin rod formation after transient common carotid artery occlusion (CCAo)

a. Panels show immunostaining for cofilin-1 (red) in the hippocampal dentate gyrus (DG), hippocampal CA1, and cerebral cortex in sections obtained at designated time points after 16 minutes of bilateral common carotid artery occlusion. Cell nuclei are stained blue. **b**. Graphs

19

585 show area of cofilin staining at each time point, expressed as percent of the image area. (n = 3;

586 *p < 0.05 v. sham)

587

588 **Fig 5. Cofilin-actin rod formation after cardiac arrest / cardiopulmonary resuscitation**

589 **(CA/CPR)**

590 **a**. Panels show immunostaining for cofilin-1 (red) in the hippocampal dentate gyrus (DG) and

591 hippocampal CA1 in sections obtained at 30 minutes or 3 hours after 8 minutes of cardiac

592 arrest. Cell nuclei are stained blue. **b**. Graphs show area of cofilin staining at each time point,

593 expressed as percent of the image area. (n = 3; *p < 0.05 v. sham)

594

595 **Fig 6. Cofilin-actin rod formation in photothrombotic permanent ischemia**

596 **a**. Representative brain section immunostained for NeuN, showing location (white box) of

597 photographs obtained. **b**. Cofilin-1 immunostaining (red) in the peri-infarct cortex at the

598 designated time points after photothrombotic vascular occlusion. White line denotes infarct

599 edge, and cell nuclei are stained blue. **c**. Lower power view of infarct edge, showing IgG

600 retention in blood vessels (green) used to define the area of photothrombosis. Cofilin-actin rods

601 (red) are formed at the edge of the infarct and extend into the non-ischemic tissue, but are not

602 formed in the core of the photothrombosed area.   **d**. Graph shows area of cofilin staining at

603 each time point, expressed as percent of the image area. (n = 3-4; *p< 0.05 v. sham).

604

605 **Fig 7. Reciprocal changes in cofilin-1 and phospho-cofilin-1 during rod formation.**

606 **a**. Immunostaining for total cofilin-1 (red) and serine-3-phospho-cofilin-1 (p-cofilin-1; green) in

607 primary neuron cultures following 1 hour of chemical oxygen-glucose deprivation (cOGD) or

608 medium exchange only (Control). Absolute intensity of the total cofilin-1 signal was in all cases

609 much greater than the p-cofilin-1 signal, and in order to show double labeling the photograph

610 settings were adjusted so that brightness of the cofilin-1 and p-cofilin-1 signals were comparable

611 under control conditions. Nuclei are stained blue with DAPI in the merged image. Magnified

612 views show neuronal processes. **b**. Fluorescence intensity of total cofilin-1 and p-cofilin-1 as

613 measured along line segments drawn orthogonal to neuronal processes, as pictured in yellow in

614 the magnified views of (**a**). Measurements were made in 10 neurites in cOGD – treated cultures

615 that contained cofilin-actin rods, and 10 neurites in control cultures (that did not have rods).

616 Note different Y-axis values in the two graphs. **c**. Aggregated peak fluorescence intensities in

617 neurites measured as in (**b**). Note different Y- axis scales in the two graphs. n = 10 neurites; **p

618 < 0.01. **d**. Confocal image from mouse brain fixed 24 hours after a 30-minute MCA occlusion,

619   with double labeling for total cofilin-1 (red) and p-cofilin-1 (green). **e**. Measurement of total

620   cofilin-1 and p-cofilin-1 immunoreactivity across cofilin-actin rods in post-ischemic brain sections

621   shows reduced p-cofilin-1 signal at the sites of cofilin-actin rod formation. n = 29 neurites

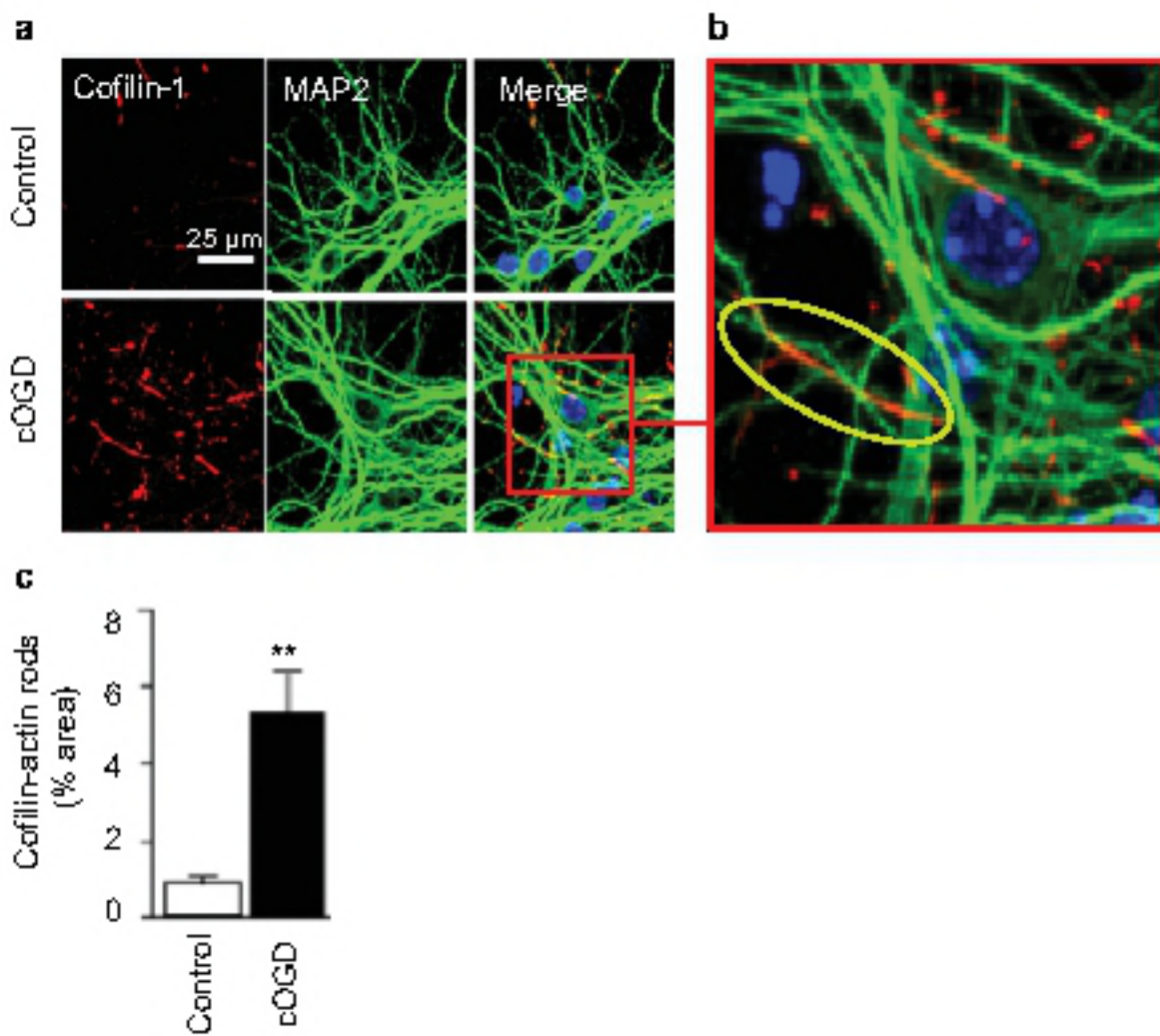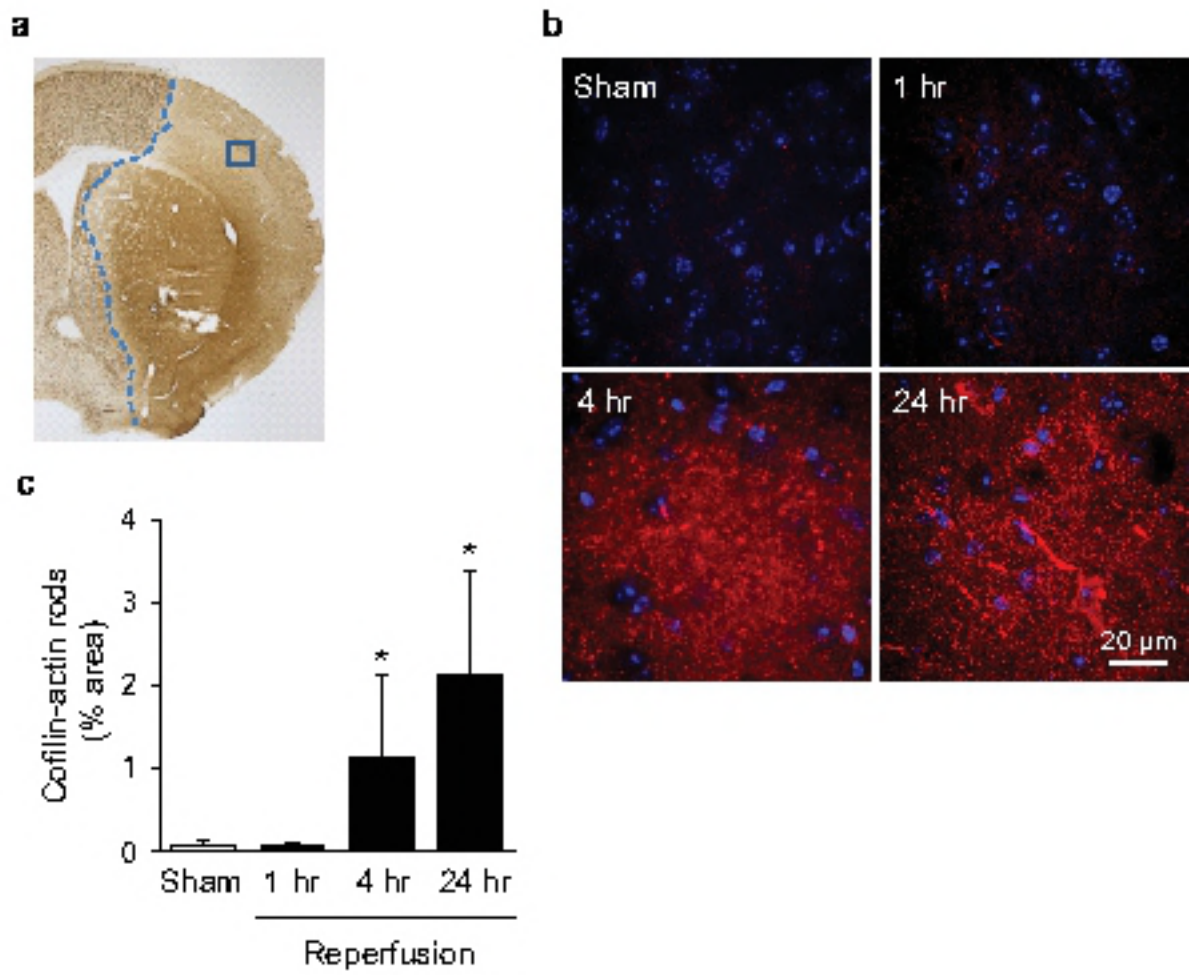622   analyzed (from 3 brains).

Figure 1

a

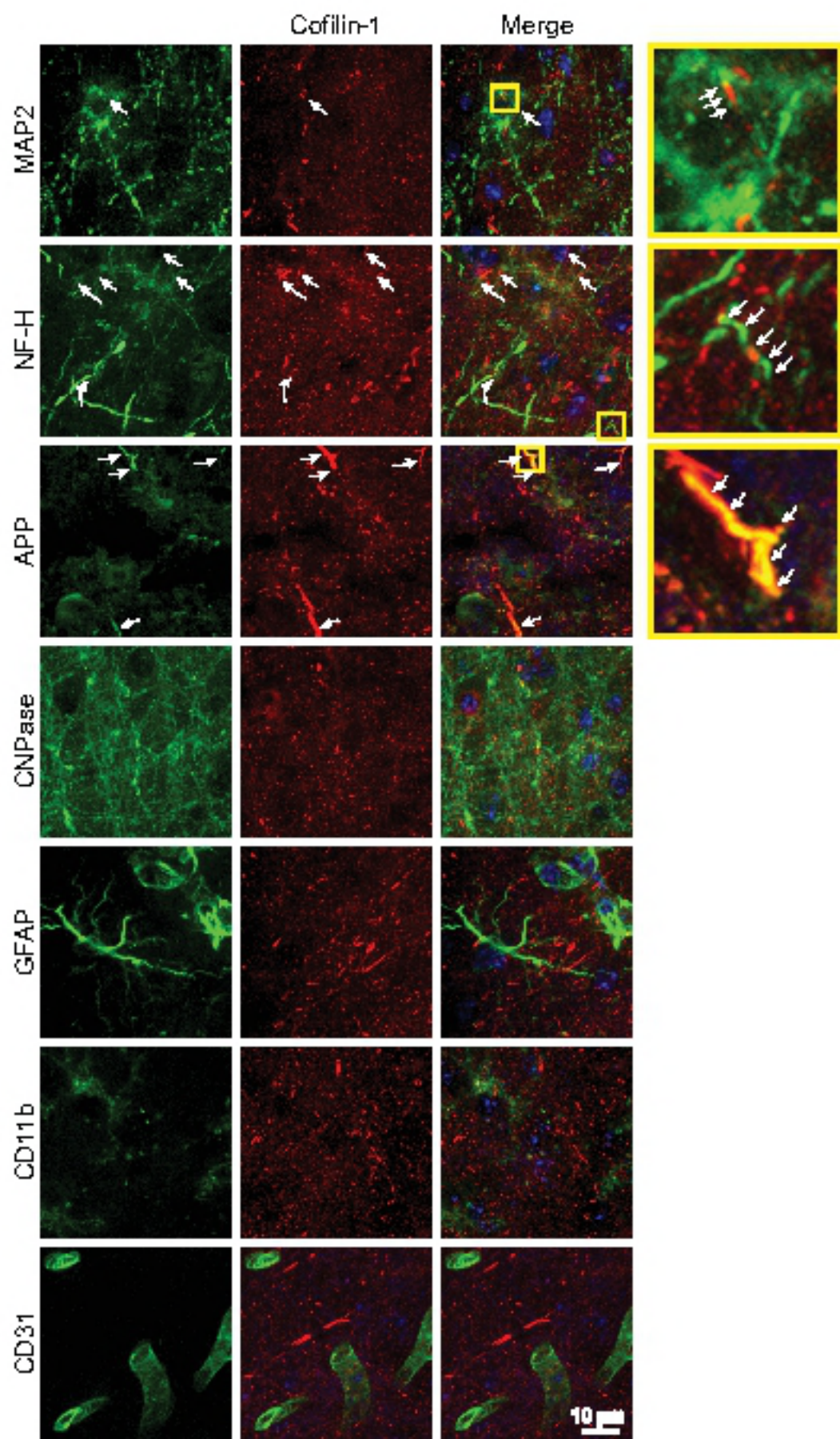|	Cofilin-1	MAP2	Merge
Control			
cOGD			

25 μm

b

c

Cofilin-actin rods (% area)

**

Control cOGD

Figure 2

a

b

Sham | 1 hr

4 hr | 24 hr

20 µm

c

Cofilin-actin rods
(% area)

Sham | 1 hr | 4 hr | 24 hr

Reperfusion

Figure 3

Figure 4

a

	Sham	0 hr	1 hr	24 hr
Dentate Gyrus				
CA1				
Cortex				

50 μm

b

DG

CA1

Cortex

Cofilin-actin rods (% area)

Sham | 0 hr | 1 hr | 24 hr
Reperfusion

Figure 5

a

	Sham	0.5 hr	3 hr
Dentate Gyrus			
CA1			20 μm

b

DG

CA1

Figure 6

Figure 7

a Cofilin-1 | p-Cofilin-1 | Merge

Control

cOGD

50 µm

25 µm

25 µm

b

Control

cOGD (cofilin-actin rods)

p-Cofilin-1
Cofilin-1

Fluorescence intensity

Distance (µm)

c

Cofilin-1

p-Cofilin-1

Peak intensity

Control | cOGD

**

**

d

10 µm

e

p-Cofilin-1
Cofilin-1

Intensity of p-Cofilin-1

Intensity of Cofilin-1

Distance (µm)